Monthly Notices
of the
ROYAL ASTRONOMICAL SOCIETY

Mon. Not. R. Astron. Soc. **422,** 106–116 (2012) doi:10.1111/j.1365-2966.2012.20559.x

A consistent comparison of bias models using observational data

A. Papageorgiou,[1,2] M. Plionis,[1,3★] S. Basilakos[4,5] and C. Ragone-Figueroa[6]

[1]*Institute of Astronomy & Astrophysics, National Observatory of Athens, Palaia Penteli, 152 36 Athens, Greece*
[2]*Faculty of Physics, Department of Astrophysics, Astronomy & Mechanics, University of Athens, Panepistemiopolis, Athens 157 83, Greece*
[3]*Instituto Nacional de Astrofísica Optica y Electrónica, AP 51 y 216, 72000 Puebla, Mexico*
[4]*Academy of Athens, Research Center for Astronomy & Applied Mathematics, Soranou Efesiou 4, 11527 Athens, Greece*
[5]*High Energy Physics Group, Department ECM, Universitat de Barcelona, Av. Diagonal 647, E-08028 Barcelona, Spain*
[6]*Instituto de Astronomía Teórica y Experimental, IATE, CONICET-Observatorio Astronómico, Universidad Nacional de Córdoba, Laprida 854, X5000BGR Córdoba, Argentina*

Accepted 2012 January 13. Received 2012 January 4; in original form 2011 November 25

ABSTRACT

We investigate five different models for the dark matter (DM) halo bias, that is, the ratio of the fluctuations of mass tracers to those of the underlying mass, by comparing their cosmological evolution using optical quasar (QSO) and galaxy bias data at different redshifts, consistently scaled to the *WMAP7* cosmology. Under the assumption that each halo hosts one extragalactic mass tracer, we use a χ^2-minimization procedure to determine the free parameters of the bias models as well as to statistically quantify their ability to represent the observational data. Using the Akaike information criterion we find that the model that represents best the observational data is the Basilakos & Plionis model with the tracer merger extension. The only other statistically equivalent model, as indicated by the same criterion, is the Tinker *et al.* model. Finally, we find an average, over the different models, DM halo mass that hosts optical QSOs of $M_{\rm h} \simeq 2.7(\pm 0.6) \times 10^{12}\, h^{-1}\, {\rm M}_{\odot}$, while the corresponding value for optical galaxies is $M_{\rm h} \simeq 6.3(\pm 2.1) \times 10^{11}\, h^{-1}\, {\rm M}_{\odot}$.

Key words: galaxies: haloes – quasars: general – cosmology: theory – large-scale structure of Universe.

1 INTRODUCTION

It is of paramount importance for cosmological and galaxy formation studies the understanding of how galaxies and other extragalactic mass tracers relate to the underlying distribution of matter. The current galaxy formation paradigm assumes that galaxies form within dark matter (DM) haloes, identified as high peaks of an underlying initially Gaussian density fluctuation field, and that they trace in a biased manner such a field (e.g. Kaiser 1984; Bardeen *et al.* 1986). A formation process of this sort can explain the difference in clustering amplitude between the different extragalactic mass tracers (galaxies, groups and clusters of galaxies, active galactic nuclei, etc.) as being due to the different bias among the underlying density fields and that of the DM haloes that host the mass tracers.

In order to quantify such a difference, one can use the so-called linear bias parameter b, which for continuous density fields is defined as the ratio of the fluctuations of the mass tracer ($\delta_{\rm tr}$) to those of the underlying mass ($\delta_{\rm m}$):

$$b = \frac{\delta_{\rm tr}}{\delta_{\rm m}}\,. \tag{1}$$

Based on this definition one can write the bias parameter in a number of equivalent ways: (a) as the square root of the ratio of the two-point correlation function of the tracers to the underlying mass:

$$b = \left(\frac{\xi_{\rm tr}}{\xi_{\rm m}}\right)^{1/2}\,, \tag{2}$$

since $\xi(r) = \langle \delta(\boldsymbol{x})\delta(\boldsymbol{x}+\boldsymbol{r})\rangle$, in which case one considers the large-scale correlation function (i.e. scales $\gtrsim 1\, h^{-1}$ Mpc), corresponding roughly to the so-called halo–halo term of the DM halo correlation function (e.g. Hamana, Yoshida & Suto 2002), and (b) as the ratio of the variances of the tracer and underlying mass density fields, smoothed at some linear scale traditionally taken to be $8\, h^{-1}$ Mpc (at which scale the variance is of the order of unity):

$$b = \frac{\sigma_{8,{\rm tr}}}{\sigma_{8,{\rm m}}}\,, \tag{3}$$

since $\sigma_8^2 = \xi(0) = \langle \delta^2(\boldsymbol{x})\rangle$.

A further important ingredient in theories of structure formation is the cosmological evolution of the DM halo bias parameter (e.g. Mo & White 1996; Tegmark & Peebles 1998, etc.). A large number of such bias evolution models have been presented in the literature and the aim of this work is to compare them using as a criterion how well do they fit the observed bias, at different redshifts, of optical QSOs and galaxies. In such a comparison we will make the

★E-mail: mplionis@astro.noa.gr

© 2012 The Authors
Monthly Notices of the Royal Astronomical Society © 2012 RAS

Downloaded from https://academic.oup.com/mnras/article-abstract/422/1/106/1019897 by Instituto Nacional de Astrofisica, Optica y Electronica user on 25 October 2018

simplified assumption that each DM halo hosts one mass tracer. This is consistent with the definition of the linear bias, where one uses either the large-scale correlation function (which corresponds to the halo–halo term) or the smoothed to linear scales variance of the fluctuation field, while any residual non-linearities will probably be suppressed in the ratio of the tracer to underlying mass correlation functions or variances. Further suppression of non-linearities, introduced, for example, by redshift-space distortions, can be archived using the integrated correlation function within some spatial scale (see discussion in Section 2 below).

There are two basic families of analytic bias evolution models. The first, called the *galaxy merging* bias model, utilizes the halo mass function and is based on the Press & Schechter (1974) formalism, the peak-background split (Bardeen *et al.* 1986) and the spherical collapse model (Cole & Kaiser 1989; Mo & White 1996, Matarrese *et al.* 1997; Moscardini *et al.* 1998; Sheth & Tormen 1999; Valageas 2009, 2011). Cole & Kaiser (1989) found for the bias evolution that

$$b(M, z) = 1/(1 + z) - 1/\left[1.68(1 + z)\right] + 1.68(1 + z)/\sigma^2(M) ,$$

where $\sigma^2(M)$ is the variance of the mass fluctuation field, while Mo & White (1996) derived for an Einstein–de Sitter universe that

$$b(z) = 0.41 + [b(0) - 0.41]\,(1 + z)^2 .$$

Mo, Jing & White (1997) extended the previous study in the quasi-linear regime by taking into account high-order correlations of peaks and haloes. Similarly, Matarrese *et al.* (1997) estimated the bias in a merging model where the halo mass exceeds a certain threshold. They found that for an Einstein–de Sitter universe

$$b(z) = 0.41 + [b(0) - 0.41]\,(1 + z)^{\beta} ,$$

while Moscardini *et al.* (1998) generalized the above bias evolution model for a variety of cosmological models.

Many studies have compared the prediction of the *merging* bias model with numerical simulations and beyond an overall good agreement, differences have been found in the details of the halo bias. For example, the spherical collapse model underpredicts the halo bias for low-mass haloes and fails to reproduce the DM halo mass function found in simulations. To solve this problem, Sheth, Mo & Tormen (2001, hereafter SMT) extended their original model to include the effects of ellipsoidal collapse. However, according to Tinker *et al.* (2010, hereafter TRK), this model underpredicts the clustering of high-peak haloes while overpredicts the bias of low-mass objects. Furthermore, Manera, Sheth & Scoccimarro (2009) and Manera & Gaztanaga (2011) find that the clustering of massive haloes cannot be reproduced from their bias calculated using the peak-background split.

Such and other differences have lead to other modifications of the models, either suggesting new fitting bias model parameters (e.g. Jing 1998, hereafter JING; Tinker, Weinberg & Zheng 2005), or new forms of the bias model fitting function (e.g. Seljak & Warren 2004; Pillepich, Porciani & Han 2010; TRK) or even a non-Markovian extension of the excursion set theory (Ma *et al.* 2011, hereafter MMRZ). A further step was provided by de Simon, Maggiore & Riotto (2011), who incorporated the effects of ellipsoidal collapse to the original MMRZ model, which is based on spherical collapse.

The second family of bias evolution models assumes a continuous mass-tracer fluctuation field, proportional to that of the underlying mass, and the tracers act as 'test particles'. In this context, the hydrodynamic equations of motion and linear perturbation theory are applied. This family of models can be divided into two subfamilies:

(a) The so-called *galaxy conserving* bias model uses the continuity equation and the assumption that tracers and the underlying mass share the same velocity field (Nusser & Davis 1994; Fry 1996; Tegmark & Peebles 1998; Hui & Parfey 2008; Schaefer, Douspis & Aghanim 2009). Then the bias evolution is given as the solution of a first-order differential equation, and Tegmark & Peebles (1998) derived

$$b(z) = 1 + [b(0) - 1]/D(z) ,$$

where $b(0)$ is the bias factor at the present time and $D(z)$ is the growing mode of density perturbations. However, this bias model suffers from two fundamental problems: *the unbiased problem*, that is, the fact that an unbiased set of tracers at the current epoch remains always unbiased in the past, and *the high-redshift problem*, that is, the fact that this model represents correctly the bias evolution only at relatively low redshifts $z \lesssim 0.5$ (Bagla 1998). Note that Simon (2005) has extended this model to also include an evolving mass-tracer population in a Λ cold dark matter (ΛCDM) cosmology.

(b) An extension of the previous model, based on the basic differential equation for the evolution of linear density perturbations, which implicitly uses that mass tracers and the underlying mass share the same gravity field and on the assumptions of linear and scale-independent bias provides a second-order differential equation for the bias. Its approximate solution provides the functional form for the cosmological evolution of bias (Basilakos & Plionis 2001, 2003; Basilakos, Plionis & Ragone-Figueroa 2008, hereafter BPR). The provided solution applies to cosmological models, within the framework of general relativity, with a dark energy equation-of-state parameter being independent of cosmic time (i.e. quintessence or phantom). An extension of this model to engulf also time-dependent dark energy equation-of-state models, including modified gravity models (geometric dark energy), was recently presented in Basilakos, Plionis & Pouri (2011).

The outline of this paper is as follows. In Section 2, we present the data that we will use, we review the basic techniques used in measuring the bias from samples of extragalactic objects and we will present the rescaling method used in order to transform different bias data to the same (*WMAP7*) cosmology (i.e. flat ΛCDM with $\Omega_{\rm m} = 0.273$ and $\sigma_8 = 0.81$). In Section 3, we introduce the different bias evolution theoretical models that we will investigate, while in Section 4 we present our results and discussion. The main conclusions are presented in Section 5. In the appendix, we discuss the simulations used to fit the free parameters of the BPR model, as well as the cosmological dependence of these parameters.

2 MASS-TRACER BIAS DATA

The mass tracers that we will use in this work are optical QSOs and galaxies, for which their linear bias with respect to the underlying mass is available as a function of redshift. In particular, we will use the following:

(i) The 2dF-based QSO results of Croom *et al.* (2005), which are based on spectroscopic data of over 20 000 QSOs covering the redshift range $0.3 \leq z \leq 2.2$ and on a ΛCDM cosmology with $\Omega_{\rm m} = 0.27$ and $\sigma_8 = 0.84$.

(ii) The SDSS (DR5) QSO ($z \lesssim 2.2$) results of Ross *et al.* (2009) based on spectroscopic data of $\sim$30 000 QSOs and and on a ΛCDM cosmology with $\Omega_{\rm m} = 0.237$ and $\sigma_8 = 0.756$.

(iii) The SDSS (DR5) QSO results of Shen *et al.* (2009), who used a homogeneous sample of $\sim$38 000 QSOs within $0.1 \leq z \leq 5$ and on a ΛCDM cosmology with $\Omega_{\rm m} = 0.26$ and $\sigma_8 = 0.78$. In this

Downloaded from https://academic.oup.com/mnras/article-abstract/422/1/106/1019897 by Instituto Nacional de Astrofisica, Optica y Electronica user on 25 October 2018

case, we will use only their $z \gtrsim 2.2$ results to avoid including in our analysis correlated measurements of the bias, for the redshift range covered also by the Ross *et al.* analysis.

Although there are other QSO bias data available, like the Myers *et al.* (2006) analysis of 300 000 photometrically classified SDSS DR4 QSOs, within $0.75 \leq z \leq 2.8$, we do not include them in our analysis in order to avoid, in the redshift range studied, as much as possible correlated bias measurements.

As far as galaxy data are concerned, we will use the bias results of Marinoni *et al.* (2005), which are based on 3448 galaxies from the VIMOS-VLT Deep Survey, cover the redshift range $0.4 \leq z \leq 1.5$ and use a ΛCDM cosmology with $\Omega_{\rm m} = 0.3$ and $\sigma_8 = 0.9$.

Although in the next section we sketch the usual procedures used to estimate the linear bias of a sample of extragalactic mass tracers, we would like to stress that for the QSO data used in this work, the corresponding authors, in order to minimize non-linear effects, have estimated the integrated correlation function for scales $>1\,h^{-1}$ Mpc, which in the usual jargon corresponds roughly to the halo–halo term of the DM halo correlation function. As for the VVTS galaxy bias data, Marinoni *et al.* devised a procedure to estimate the bias of a smooth galaxy density field in pencil beam surveys, disentangling the non-linear effects, and thus the bias values used in this work correspond to the linear bias.

2.1 Estimating the tracer bias at different redshifts

Although we will use the bias data provided by the previous references, for completion, we briefly present here the basic methodology used to estimate the bias of some extragalactic mass tracer at a redshift interval $z \pm \delta z$, using any of the basic definitions of equations (1)– (3).

The first issue that one has to keep in mind is that what we measure from redshift catalogues is the redshift-space distorted value of either the tracer correlation function, $\xi_{\rm tr}(s)$, or the variance of the tracer density field $\sigma^2_{8,{\rm tr},s}$ (the index s indicates redshift-space distorted spatial separations, while the index 'tr' indicates true spatial separations). One needs to correct for such distortions, resulting from the peculiar velocities of the mass tracers, in order to recover the true spatial value of either measure. Kaiser (1987) provides such a correction procedure which entails in dividing the directly measured, from observational data tracer correlation function or variance with a function $F(\Omega_{\rm m}, \Omega_\Lambda, b, z)$, given by (see also Hamilton 1998; Marinoni *et al.* 2005)

$$F(\Omega_{\rm m}, \Omega_\Lambda, b, z) = 1 + \frac{2}{3}\beta(z) + \frac{1}{5}\beta^2(z) \tag{4}$$

with $\beta(z) = \Omega_{\rm m}^{\gamma}(z)/b(z)$, and $\gamma = 6/11$ for the ΛCDM (e.g. Wang & Steinhardt 1998; Linder 2005), which implies that $\beta(z) = \Omega_{\rm m}^{6/11} E(z)^{-12/11}(1+z)^{18/11}/b(z)$. Therefore, the relation between the redshift-space and real-space measures used to estimate the bias parameter is

$$\frac{\xi_{\rm tr}(s,z)}{\xi_{\rm tr}(r,z)} = \frac{\sigma^2_{8,{\rm tr},s}(z)}{\sigma^2_{8,{\rm tr},r}(z)} = F(\Omega_{\rm m}, \Omega_\Lambda, b, z). \tag{5}$$

Then combining equation (2) or (3) with equations (4) and (5) provides the real-space bias factor according to

$$b(z) = \left[\frac{\xi_{\rm tr}(s,z)}{\xi_{\rm m}(r,z)} - \frac{4\Omega_{\rm m}^{12/11}(z)}{45}\right]^{1/2} - \frac{\Omega_{\rm m}^{6/11}(z)}{3},$$
$$= \left[\frac{\sigma^2_{8,{\rm tr},s}(z)}{\sigma^2_{8,{\rm m}}(z)} - \frac{4\Omega_{\rm m}^{12/11}(z)}{45}\right]^{1/2} - \frac{\Omega_{\rm m}^{6/11}(z)}{3}, \tag{6}$$

where $\xi_{\rm m}(r)$ and $\sigma^2_{8,{\rm m}}$ are the corresponding correlation function and variance of the underlying DM distribution, given by the Fourier transform of the spatial power spectrum $P(k)$ of the matter fluctuations, linearly extrapolated to the present epoch:

$$\xi_{\rm m}(r,z) = \frac{D^2(z)}{2\pi^2}\int_0^\infty k^2 P(k)\frac{\sin(kr)}{kr}{\rm d}k \tag{7}$$

and

$$\sigma^2_{8,{\rm m}}(z) = \frac{D^2(z)}{2\pi^2}\int_0^\infty k^2 P(k) W^2(kR_8){\rm d}k, \tag{8}$$

with $D(z)$ the normalized perturbation's growing mode [i.e. such that $D(0) = 1$], $P(k)$ the CDM power spectrum given by

$$P(k) = P_0 k^n T^2(\Omega_{\rm m}, k)\,, \tag{9}$$

with $T(\Omega_{\rm m}, k)$ being the CDM transfer function (Bardeen *et al.* 1986; Sugiyama 1995; Eisentein & Hu 1998), n the slope of the primordial power spectrum (which according to *WMAP7* is $= 0.967$) and $W(kR_8)$ the Fourier transform of the top-hat smoothing kernel of radius $R = R_8 = 8h^{-1}$ Mpc, given by $W(kR_8) = 3(\sin kR_8 - kR_8\cos kR_8)/(kR_8)^3$.

Now, although in the case of using equation (3), the σ_8 variance is free of non-linear effects by definition, this is not so when using the correlation function approach (equation 2). Therefore, in order to minimize non-linear effects at small separations, one can replace $\xi_{\rm tr}(s)$ in equation (6) with the integrated correlation function, $\bar{\xi}_{\rm tr}(s)$.

An alternative approach in order to avoid redshift-space distortions is to resolve the redshift-space separation, s, into two components, one perpendicular ($r_{\rm p}$) and one parallel (π) to the line of sight (see Davis & Peebles 1983) and then estimating the two-point projected correlation function $w_{\rm p}(r_{\rm p})$ along the perpendicular dimension (within some range of the parallel dimension, say, $\pi_{\rm min} < \pi < \pi_{\rm max}$), which is related to the spatial correlation function, $\xi(r)$, according to

$$w_{\rm p}(r_{\rm p}) = \int_{\pi_{\rm min}}^{\pi_{\rm max}} \xi(r_{\rm p}, \pi)\,{\rm d}\pi = \int_{\pi_{\rm min}}^{\pi_{\rm max}} \frac{r\xi(r)}{\sqrt{r^2 - r_{\rm p}^2}}{\rm d}r, \tag{10}$$

where $\pi = |\Delta d|$ and $r_{\rm p} = \Delta d \tan\theta/2$, with Δd the radial comoving distance separation of any pair of mass tracers and θ is angular separation on the sky of the pair members. As before, one can use the integrated correlation function, $\bar{\xi}$, in order to minimize non-linear effects.

Additionally, one can also use the angular two-point correlation function, $w(\theta)$, instead of $\xi(s)$ or $w_{\rm p}(r_{\rm p})$, in order to obtain $\xi(r)$ via Limber's inversion, a procedure which also avoids the peculiar velocity distortions, but is hampered by the necessity of a priori knowing the redshift selection function of the mass tracers.

2.2 Scaling the bias data to the same cosmology

Since different authors have estimated the optical QSO and galaxy bias using different cosmologies, we need to convert them to the same cosmological background in order to be able to use them consistently. As such we choose the recent *WMAP7* cosmology (Komatsu *et al.* 2011).

The procedure that we will follow uses the different σ_8 power spectrum normalizations (equation 3). We wish to translate the value of bias from one cosmological model, say, B, to another, say, A. The definition of bias at a redshift z for these two different cosmologies is given by

$$b_A(z) = \frac{\sigma_{8,{\rm tr},r,A}(z)}{\sigma_{8,{\rm m},A}(z)} \tag{11}$$

Downloaded from https://academic.oup.com/mnras/article-abstract/422/1/106/1019897 by Instituto Nacional de Astrofisica, Optica y Electronica user on 25 October 2018

and

$$b_B(z) = \frac{\sigma_{8,\mathrm{tr},r,B}(z)}{\sigma_{8,\mathrm{m},B}(z)} \tag{12}$$

where the numerator is the real-space value of $\sigma_8(z)$ estimated directly from the data, using also equation (5) to correct for redshift-space distortions. Dividing now equation (11) by (12), taking into account equation (5), and making the fair assumption that

$$\sigma_{8,\mathrm{tr},s,A}(z) \simeq \sigma_{8,\mathrm{tr},s,B}(z)\ , \tag{13}$$

since the different cosmologies enter only weakly in the observational determination of $\sigma_{8,\mathrm{tr}}$, through the definition of distances, we then have

$$b_A(z) \simeq b_B(z)\frac{\sigma_{8,\mathrm{m},B}(z)}{\sigma_{8,\mathrm{m},A}(z)}\left[\frac{F(\Omega_{\mathrm{m},B},\,\Omega_{\Lambda,B},\,b_B,\,z)}{F(\Omega_{\mathrm{m},A},\,\Omega_{\Lambda,A},\,b_A,\,z)}\right]^{1/2}\ . \tag{14}$$

As it can be realized the required rescaled real-space bias, b_A, enters also in the right-hand side of the above equation, making it rather complicated to analytically derive the full expression (using for example equation 6). However, noting that the redshift-space distortion correction enters in the scaling of the bias, from one cosmology to another, as the square root of the ratio of the F functions, the expected deviation by using in the right-hand side of equation (14) the crude approximation $b_A \simeq b_B$ does not affect significantly this correction. In any case, the magnitude of the relevant correction, $(F_B/F_A)^{1/2}$, is extremely small, typically $\sim$0.8 per cent at $z = 0.24$ dropping to $\sim$0.1 per cent at $z = 2.1$, and the overall scaling of the bias to different cosmologies is dominated by the ratio of the corresponding $\sigma_8(z)$ variances.

We can facilitate our scaling procedure by using the $\sigma_8(z = 0)$ power spectrum normalizations of the different models, a value always provided by the different authors. We therefore translate the values of $\sigma_8(z)$ to that at $z = 0$ by using the linear growing mode of perturbations according to $\sigma_8(z) = \sigma_8(0)D(z)$. The final scaling relation from the B cosmology to that of A therefore becomes

$$b_A(z) \simeq b_B(z)\frac{\sigma_{8,\mathrm{m},B}(0)}{\sigma_{8,\mathrm{m},A}(0)}\frac{D_B(z)}{D_A(z)}\left[\frac{F(\Omega_{\mathrm{m},B},\,\Omega_{\Lambda,B},\,b_B,\,z)}{F(\Omega_{\mathrm{m},A},\,\Omega_{\Lambda,A},\,b_B,\,z)}\right]^{1/2}\ . \tag{15}$$

3 THEORETICAL BIAS MODELS

Here we briefly describe the bias evolution models that we are going to compare. As discussed in the introduction, we separate the models in two families. The *galaxy merging model* family, based on the Press–Schether formalism and the peak-background split. The models that we will investigate, representing this family, are the SMT extension of the original Sheth & Tormen (1999) model (SMT model), the JING model, the TRK model and the MMRZ model. All these models provide the bias of haloes as a function of the peak-height parameter, ν, where

$$\nu \equiv \delta_{\mathrm{c}}(z)/\sigma(M_{\mathrm{h}},\,z)\ , \tag{16}$$

with M_{h} the halo mass, $\sigma^2(M_{\mathrm{h}},\,z)$ the variance of the mass fluctuation field at redshift z, and $\delta_{\mathrm{c}}(z)$ the critical linear overdensity for spherical collapse, which has a weak redshift dependence (see equation 18 of Weinberg & Kamionkowski 2003).

The basic free parameter of these bias models, to be fitted by the data (although depending on the model one more parameter may be allowed to vary – see below), is ν and through the evolution of $\sigma(M_{\mathrm{h}},\,z)$ we will be able to derive the predicted bias redshift evolution, as well as the value of M_{h}. The latter value will be estimated by using the definition of σ, equations (8) and (9), from which we have that

$$\sigma^2(M_{\mathrm{h}}) = \sigma_8^2\,\frac{\int_0^\infty \mathrm{d}k k^{n+2}T^2(k)W^2(kR)}{\int_0^\infty \mathrm{d}k k^{n+2}T^2(k)W^2(kR_8)}\ , \tag{17}$$

with $R = (3M_{\mathrm{h}}/4\pi\bar{\rho})^{1/3}$, $R_8 = 8\,h^{-1}\,\mathrm{Mpc}$ and $\bar{\rho} = 2.78 \times 10^{11}\,\Omega_{\mathrm{m}}\,h^2\,\mathrm{M}_\odot\,\mathrm{Mpc}^{-3}$.

The second family contains the so-called *galaxy conserving* models and their extensions. These models are based on the hydrodynamical equations of motion and linear perturbation theory while the most general such model, which we will investigate, is that of Basilakos & Plionis (2001, 2003), extended to included a correction for halo merging in BPR.

Below we present the functional form of the bias evolution for each of the models that we will investigate.

3.1 BPR model

Basilakos & Plionis (2001, 2003) using linear perturbation theory and the Friedmann–Lemaitre solutions derived a second-order differential equation for the evolution of bias, assuming that the mass-tracer population is conserved in time and that the tracer and the underlying mass share the same dynamics.

The solution of their differential equation, for a flat cosmology, was found to be (Basilakos & Plionis 2001)

$$b(z) = C_1E(z) + C_2E(z)I(z) + 1, \tag{18}$$

where $E(z) = [\Omega_{\mathrm{m}}(1+z)^3 + \Omega_\Lambda]^{1/2}$ and

$$I(z) = \int_z^\infty \frac{(1+x)^3}{E^3(x)}\mathrm{d}x\ . \tag{19}$$

The constants of integration depend on the halo mass, as shown in BPR, and they are given by

$$C_1(M_{\mathrm{h}}) \approx \alpha_1\left(\frac{M_{\mathrm{h}}}{10^{13}\,h^{-1}\,\mathrm{M}_\odot}\right)^{\beta_1}, \tag{20}$$

$$C_2(M_{\mathrm{h}}) \approx \alpha_2\left(\frac{M_{\mathrm{h}}}{10^{13}\,h^{-1}\,\mathrm{M}_\odot}\right)^{\beta_2}, \tag{21}$$

and the values of $\alpha_{1,2}$ and $\beta_{1,2}$ were estimated originally from an $\sim$*WMAP1* ΛCDM numerical simulation in BPR. We have since run a *WMAP7* ΛCDM simulation, the details of which can be found in Appendix A1, and from which we have determined the new values of the $\alpha_{1,2}$ and $\beta_{1,2}$ parameters (see Table A1). The cosmological dependence of these parameters is also discussed in Appendix A2.

In BPR it was found that the original Basilakos & Plionis model could well reproduce the bias evolution for $z < 3$, but not at higher redshifts, indicating the necessity to extend the model to include the contribution of an evolving mass-tracer population. Such an extension was presented in BPR and it was based on a phenomenological approach, although the functional form for the effects of merging was based on physically motivated arguments (see appendix A2 of BPR). To this end they introduced to the continuity equation an additional time-dependent term, $\Psi(t)$, associated with the effects of merging of the mass tracers, which depends on the tracer number density, its logarithmic derivative and on δ_{tr}. They parametrized this term using a standard evolutionary form

$$\Psi(z) = AH_0(1+z)^\mu, \tag{22}$$

where μ and A are positive parameters which engulf the (unknown) physics of galaxy merging. The bias evolution is now given by

$$b(z) = C_1E(z) + C_2E(z)I(z) + y_{\mathrm{p}}(z) + 1, \tag{23}$$

Downloaded from https://academic.oup.com/mnras/article-abstract/422/1/106/1019897 by Instituto Nacional de Astrofisica, Optica y Electronica user on 25 October 2018

where the additional halo-merging factor, $y_p(z)$, is given by

$$y_p(z) = E(z)\int_0^z \tau(x)I(x)\,dx - E(z)I(z)\int_0^z \tau(x)\,dx \quad (24)$$

with $\tau(z) = f(z)E^2(z)/(1+z)^3$ and $f(z) = A(\mu-2)(1+z)^\mu E(z)/D(z)$. The values of both A and μ have been fitted using ΛCDM numerical simulations (see BPR) and it was found that $\mu \simeq 2.5$–2.6 independent of the halo mass, while A increases with decreasing halo mass, with $A \simeq 0.006$ and 0 for intermediate (i.e. $10^{13} \lesssim M_h \lesssim 10^{13.8}\,h^{-1}\,M_\odot$) and higher mass haloes, respectively. Evidently, the bias factor at $z = 0$ is provided by

$$b(z) = C_1 + C_2 I(0) + 1\ . \quad (25)$$

Therefore, in the current analysis we will leave M_h as a free parameter to be fitted by the data (BPR model), but we will also allow the parameter α_1 to be fitted by the data, keeping A equal to its simulation-based value ($A = 0.006$, BPR-I model), as well as the parameter A to be fitted by the data keeping α_1 equal to its simulation based value ($\alpha_1 = 4.53$, BPR-II model).

3.2 SMT model

In SMT the original work of Sheth & Tormen (1999) was extended for the case of an ellipsoidal, rather than a spherical collapse. This new ingredient reduces the difference between theoretical expectations and simulation DM halo data. Considering ellipsoidal collapse, the density threshold required for collapse, contrary to the spherical collapse case, depends on the mass of the final object.

Using the ratio of the halo power spectrum to that of the underlying mass, they derived the functional form for the bias as

$$b(\nu) = 1 + \frac{1}{\sqrt{a}\delta_c(z)}\left[\sqrt{a}(a\nu^2) + \sqrt{a}b(a\nu^2)^{1-c} - f(\nu)\right]$$
$$\text{with}\quad f(\nu) = \frac{(a\nu^2)^c}{(a\nu^2)^c + b(1-c)(1-c/2)}\ , \quad (26)$$

where the free parameters were evaluated using N-body simulations to have values $a = 0.707$, $b = 0.5$ and $c = 0.6$. In particular the value of a was found to depend mostly on how the simulation DM haloes were identified. In the case of a Friends-of-Friends (FoF) algorithm the value $a = 0.707$ corresponds to the standard linking length of 0.2 times the mean interparticle separation. Decreasing the linking length would increase the value of a and vice versa (see discussion in SMT). Therefore, beyond the value of the DM halo mass, M_h [which will be estimated from the resulting value of $\sigma(M_h)$ via equation (17)], we will also allow the parameter a to be fitted by the data.

3.3 JING model

JING used the clustering of simulation DM haloes to derive an expression for the bias which is independent of the shape of the initial power spectrum, being CDM or power law. His corresponding expression is

$$b(\nu) = \left(\frac{0.5}{\nu^4} + 1\right)^{(0.06-0.02n)}\left(1 + \frac{\nu^2 - 1}{\delta_c}\right)\ , \quad (27)$$

where n is the linear power spectrum index at the halo scale [i.e. $n = d\ln P(k)/d\ln k \simeq -2$ for $M_h \simeq 10^{13}\,h^{-1}\,M_\odot$]. The only free parameter of this model, to be fitted by the data, is the halo mass M_h [which will be estimated from the fitted value of $\sigma(M_h)$ via equation 17].

3.4 TRK model

TRK measure the clustering of DM haloes based on a large series of collisionless N-body simulations of the ΛCDM cosmology. DM haloes were identified using the spherical overdensity algorithm by which haloes are considered as isolated peaks in the density field such that the mean density is Δ times the density of the background. Their bias fitting function reads

$$b(\nu) = 1 - A\frac{\nu^a}{\nu^a + \delta_c^a} + B\nu^b + C\nu^c\ , \quad (28)$$

where $y = \log_{10}\Delta$. For the *WMAP7* ΛCDM model, the value which corresponds to the virialization limit is $\Delta_{\Lambda CDM} \simeq 355$. The rest of the parameters of the model are $A = 1 + 0.24y\exp[-(4/y)^4]$, $B = 0.183$, $C = 0.019 + 0.107y + 0.19\exp[-(4/y)^4]$, $a = 0.44y - 0.88$, $b = 1.5$ and $c = 2.4$.

Therefore, we will fit the observational data using as a single free parameter the DM halo mass [M_h, derived via $\sigma(M_h)$ in equation 17] and using $y = \log_{10}(\Delta_{\Lambda CDM})$. However, we will also allow the latter parameter to be fitted by the data, simultaneously with M_h.

3.5 MMRZ model

MMRZ extended the original Press–Schether approach incorporating a non-Markovian extension with a stochastic barrier, where they assume that the critical value for spherical collapse is itself a stochastic variable, whose scatter reflects a number of complicated aspects of the underlying dynamics.

Their model contains two parameters: κ, which parametrizes the degree of non-Markovianity and whose exact value depends on the shape of the filter function used to smooth the density field, and α, the so-called *diffusion coefficient*, which parametrizes the degree of stochasticity of the barrier. Taking into account the non-Markovianity and the stochasticity of the barrier, the bias takes the form

$$b(\nu) = 1 + \frac{\alpha\nu^2 - 1 + \frac{\alpha\kappa}{2}\left[2 - e^{\alpha\nu^2/2}\Gamma\left(0, \frac{\alpha\nu^2}{2}\right)\right]}{\sqrt{\alpha}\delta_c\left[1 - \alpha\kappa + \frac{\alpha\kappa}{2}e^{\alpha\nu^2/2}\Gamma\left(0, \frac{\alpha\nu^2}{2}\right)\right]}, \quad (29)$$

where $\alpha = (1 + D_B)^{-1}$, with D_B the diffusion coefficient, and $\Gamma(0, x)$ the incomplete gamma function. Without the stochasticity of the barrier, one has $D_B = 0 \rightarrow \alpha = 1$.

MMRZ have found using N-body simulations that using $\alpha = 0.818$ and $\kappa = 0.23$ they can reproduce to a good extent both the simulation bias and the halo mass function as a function of ν. We will therefore use these parameter values to fit the observational bias data in order to constrain M_h. Additionally, we will allow both α and M_h to be fitted simultaneously by the data, using $\kappa = 0.44$, since this is the value for a top-hat smoothing kernel in coordinate space. Note that the value of κ appears to be almost independent of cosmology, as discussed in Maggiore & Riotto (2010).

4 FITTING MODELS TO THE DATA

In order to quantify the free parameters of the DM halo bias models, we perform a standard χ^2-minimization procedure between N bias data measurements, $b_i(z)$, with the bias values predicted by the models at the corresponding redshifts, $b(\boldsymbol{p}, z)$. The vector $\boldsymbol{p}$ represents the free parameters of the model and depending on the model their number is one or two. This procedure makes the simplistic assumption that each DM halo hosts one mass tracer, an assumption that is justified from the way the QSO and galaxy bias data have been estimated (see discussion in Section 2).

Downloaded from https://academic.oup.com/mnras/article-abstract/422/1/106/1019897 by Instituto Nacional de Astrofisica, Optica y Electronica user on 25 October 2018

The χ^2 function is defined as

$$\chi^2 = \sum_{i=1}^{N} \left[\frac{b_i(z) - b(\boldsymbol{p}, z)}{\sigma_{b_i}(z)} \right]^2 , \quad (30)$$

with $\sigma_{b_i}(z)$ is the observed bias uncertainty. We have in total $N = 22$ measured bias data for the optical QSOs, spanning from $z = 0.24$ to 4, and $N = 5$ for the optical galaxies, spanning from $z = 0.55$ to 1.4.

Note that the uncertainty of the fitted parameters will be estimated, in the case of more than one such parameter, by marginalizing one with respect to the other. However, since such a procedure may hide possible degeneracies between parameters, we will also present the 1, 2 and 3σ likelihood contours in the parameter plane.

Furthermore, since we will attempt to compare the different models among them, the χ^2 test alone is not sufficient for such a task, since different models may have a different number of free parameters. Instead we will use information criteria to compare the strengths of the different models, according to the work of Liddle (2004), a procedure that favours those models that give a similarly good fit to the data but with fewer free parameters (see e.g. Saini, Weller & Bridle 2004; Godlowski & Szydlowski 2005; Davis *et al.* 2007, and references therein). To this end we will use, relevant to our case, the *corrected* Akaike information criterion for small sample size (AIC_c; Akaike 1974; Sugiura 1978), defined, for the case of Gaussian errors, as

$$\mathrm{AIC}_c = \chi^2 + 2k + 2k(k-1)/(N-k-1), \quad (31)$$

where k is the number of free parameters, and thus when $k = 1$, $\mathrm{AIC}_c = \chi^2_{\rm min} + 2$. A smaller value of AIC_c indicates a better model–data fit. However, small differences in AIC_c are not necessarily significant and therefore in order to assess the effectiveness of the different models in reproducing the data, one has to investigate the model pair difference $\Delta\mathrm{AIC}_c = \mathrm{AIC}_{c,y} - \mathrm{AIC}_{c,x}$. The higher the value of $|\Delta\mathrm{AIC}_c|$, the higher the evidence against the model with a higher value of AIC_c, with a difference $|\Delta\mathrm{AIC}_c| \gtrsim 2$ indicating a positive such evidence and $|\Delta\mathrm{AIC}_c| \gtrsim 6$ indicating a strong such evidence, while a value $\lesssim 2$ indicates consistency between the two comparison models.

4.1 Optical QSO results

Here we fit the different bias evolution models to the scaled to the *WMAP7* cosmology optical QSO data, described in Section 2. It is important to note that all the bias models used in this work (except the BPR model) have been studied as a function of threshold ν, equation (16), that is, in effect as a function of the variance of the fluctuation field and thus as a function of halo mass, while the free parameters of most models have been fitted using $z = 0$ simulations. In these models, the redshift dependence of the bias comes mostly from the redshift dependence of the peak height, ν (see equation 16).

We will present separately the results of the models with one free parameter, the halo mass, and the models with an additional free parameter, as discussed in the theoretical model presentation sections.

4.1.1 One-free-parameter models

In Table 1, we present the best-fitting model parameters based on the χ^2-minimization procedure, with the first and second columns listing the fitted halo mass, $M_{\rm h}$, derived using equation (17) and the value of bias at $z = 0$, respectively. We also present the goodness-of-fit statistics, as discussed previously (reduced χ^2 and AIC_c). In the top panel of Fig. 1, we present the bias evolution models (different lines), using the best-fitting parameter values listed in Table 1 together with the *WMAP7*-scaled optical QSO bias data. The inset panel of Fig. 1 shows that the resulting $M_{\rm h}$ values cluster around two, relatively similar, values: $\sim 3 \times 10^{12}$ and $\sim 2 \times 10^{12}\, h^{-1}\, \mathrm{M}_\odot$. In the bottom panel, we present the relative difference between the BPR model and all the rest, that is, $\Delta b_{\rm BPR}(z) = [b_i(z) - b_{\rm BPR}(z)]/b_{\rm BPR}(z)$.

Table 1. Results of the χ^2-minimization procedure between the optical QSO data ($N = 22$) and bias models with one free parameter ($k = 1$).

Model	$10^{12}\, h^{-1}\, \mathrm{M}_\odot$	$b(0)$	$\chi^2_{\rm min}$/d.o.f.	AIC_c
BPR	3.0 ± 0.4	1.02	12.88/21	14.88
SMT	3.2 ± 0.4	1.07	23.21/21	25.21
JING	2.1 ± 0.2	0.98	18.00/21	20.00
TRK	3.0 ± 0.4	1.00	15.79/21	17.79
MMRZ	2.2 ± 0.2	0.87	20.14/21	22.14

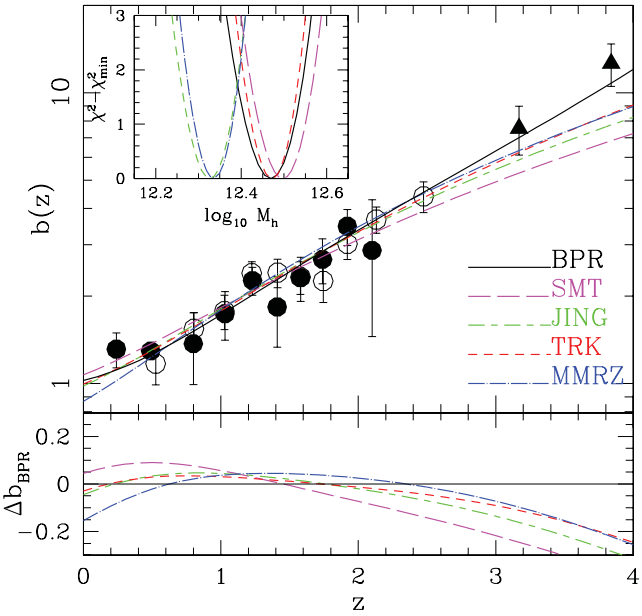

Figure 1. Top panel: comparison of the QSO bias data [open circles correspond to Croom *et al.* (2005); filled circles to Ross *et al.* (2009); and filled triangles to the high-redshift data of Shen *et al.* (2009)] with the one-free-parameter bias model fits (BPR: black continuous line; SMT: magenta dashed line; JING: green long-dashed–short-dashed line; TRK: red short-dashed line; MMRZ: blue dot–dashed line). Bottom panel: the relative difference between the BPR model and all the rest, $\Delta b_{\rm BPR}(z)$. Inset panel: the value of $\chi^2 - \chi^2_{\rm min}$ as a function of halo mass, $M_{\rm h}$, for the indicated bias models.

Some basic conclusions that become evident, inspecting also Table 1, are as follows:

(i) Although all one-free-parameter bias models appear to fit at a statistically acceptable level the optical QSO bias data, by far the best model is the BPR model, which is the only model fitting also the highest redshifts ($z \gtrsim 3$). The MMRZ model is the only model that does not fit the lowest redshifts ($z \lesssim 0.3$), providing an anti-biased value at the current epoch, $b(0) = 0.87$.

(ii) The relative bias difference of the various fitted models with respect to that of the BPR model, $\Delta b_{\rm BPR}(z)$, indicates that the BPR,

Downloaded from https://academic.oup.com/mnras/article-abstract/422/1/106/1019897 by Instituto Nacional de Astrofisica, Optica y Electronica user on 25 October 2018

JING and TRK models have a very similar redshift dependence for $z \lesssim 2.2$ (with $|\Delta b_{\rm BPR}(z)| \lesssim 0.05$), while all the models show very large such deviations for $z \gtrsim 2.8$, reaching $|\Delta b_{\rm BPR}| \gtrsim 0.3$ at the largest redshifts. The SMT and MMRZ models show large deviations at the lowest redshifts as well.

(iii) Beyond the fact that the BPR model provides by far the best fit to the QSO bias data, the second best model is the TRK model, with $\Delta{\rm AIC}_c \sim -2.9$. Furthermore, one can distinguish that the model pairs (JING, TRK) and (JING, MMRZ) are statistically equivalent ($\Delta{\rm AIC}_c \lesssim 2$).

(iv) The traditional SMT and the recently proposed MMRZ models rate the worst among all the other one-parameter models, but interestingly the former provides consistent values of $M_{\rm h}$ and $b(0)$ with those of the BPR model.

We attempt now to provide a robust average value of the DM halo mass that hosts optical QSOs, using an inverse-AIC$_c$ weighting of the different one-parameter-model results. This procedure provides a weighted mean and combined weighted standard deviation of the DM halo mass of

$$(\mu_{M_{\rm h}}, \sigma_{M_{\rm h}}) = (2.72, 0.56) \times 10^{12}\, h^{-1}\, {\rm M}_\odot,$$

while the weighted scatter of the mean is $\sim 0.44 \times 10^{12}\, h^{-1}\, {\rm M}_\odot$.

Finally, we point out that since it appears that mainly the two high-z bias points are the ones that give the advantage to the BPR model with respect to the others, we perform a more conservative comparison among the models by excluding these two high-z data points. We find that although the resulting halo mass and $b(0)$ are very similar to those of Table 1, with variations of a few per cent, there are now three models that perform equivalently well, the BPR, JING and TRK models with AIC$_c \simeq 13$. The other two models perform moderately (SMT model) or significantly (MMRZ model) worse, as was the case also in the full data comparison, with $\Delta{\rm AIC}_c \simeq 2$ and 4, respectively.

4.1.2 *Two-free-parameter models*

We now allow a second parameter to be fitted simultaneously with the DM halo mass. Since the free parameters of the bias models have been determined using N-body simulations, it would be interesting to investigate if their simulation-based value can be reproduced by real observational data. The second free parameter that we will use is α_1, A, a, y and α for the BPR-I, BPR-II, SMT-I, TRK-I and MMRZ-I models, respectively. Note that in the case of the BPR-II model we will use the simulation based value of α_1, with the free parameter A being the halo-merging parameter of the BPR model (defined in Section 3.5).

Table 2 presents the best-fitting model parameters resulting from the χ^2-minimization procedure, with the first and second columns representing, respectively, the resulting halo mass, $M_{\rm h}$, and the second free parameter, while the third column the value of the bias at $z = 0$. In the top panel of Fig. 2, we compare the resulting bias evolution models with the *WMAP7*-scaled QSO bias data (as in Fig. 1), while in the bottom panel we present the relative difference between the BPR-II model and all the rest, that is, $\Delta b_{\rm BPR\text{-}II}(z) = [b_i(z) - b_{\rm BPR\text{-}II}(z)]/b_{\rm BPR\text{-}II}(z)$.

Table 2. Results of the χ^2-minimization procedure between the optical QSO data and the bias models with two free parameters.

Model	$10^{12}\, h^{-1}\, {\rm M}_\odot$	Second parameter	$b(0)$	$\chi^2_{\rm min}$/d.o.f.	AIC$_c$
BPR-I	2.2 ± 0.4	4.64 ± 0.07	1.08	11.95/20	16.16
BPR-II	2.8 ± 0.6	0.008 ± 0.005	1.02	12.45/20	16.66
SMT-I	27.0 ± 4.0	0.40 ± 0.02	0.95	18.72/20	22.93
TRK-I	0.4 ± 0.1	6.14 ± 0.43	1.11	13.37/20	17.58
MMRZ-I	0.3 ± 0.1	1.21 ± 0.04	0.87	21.27/20	25.48

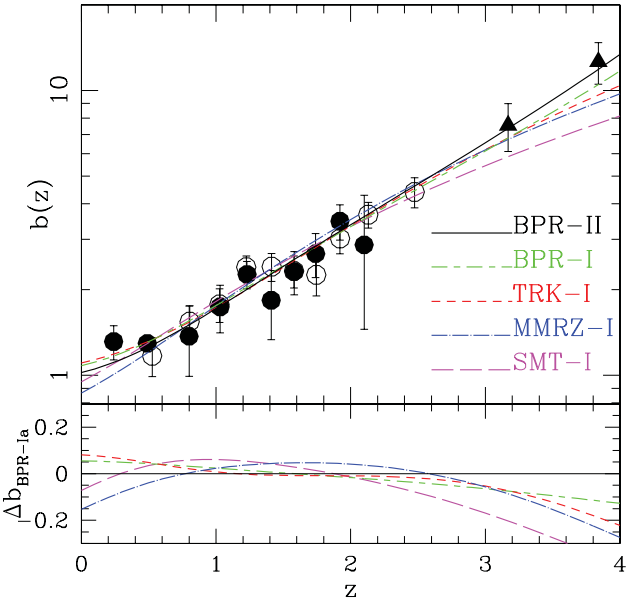

Figure 2. Top panel: comparison of the QSO bias data with the two-free-parameter bias models (their line types and colours are indicated in the figure). Bottom panel: the relative difference, $\Delta b_{\rm BPR\text{-}II}(z)$, between the BPR-II and the rest of the models.

Below we list the main conclusions of the above fitting procedure:

(i) A first important result is that the only model that reproduces the simulation-based second-free-parameter value is the BPR-I model. The simulation-based value is $\alpha_1 = 4.53$, while the fitted value, based on the QSO bias data, is $\alpha_1 = 4.64 \pm 0.07$. This fact will allow us to derive the dependence of the parameters of the BPR bias evolution model on the relevant cosmological parameters (see Appendix A2).

(ii) Fitting the BPR-II model to the QSO data provides $A = 0.008 \pm 0.005$ which is almost identical to the simulation-determined value, used in the BPR case ($A = 0.006$). As it is therefore expected, the fitted values of $M_{\rm h}$ and $b(0)$ are almost identical to those of the one-parameter BPR model, but the statistical significance of the BPR-II model is lower than that of the BPR model due to its two free parameters.

(iii) Although the SMT-I and TRK-I models appear now to fit slightly better the QSO bias data, especially the higher z range, this happens at the expense of providing unexpected values for $M_{\rm h}$ and very different values of the second fitted parameter with respect to their simulation-based value. For example, the SMT-I model provides a huge halo mass, approximately nine times larger than that provided by the corresponding one-parameter model. This should be attributed to the fact that the fitted second parameter, a, is significantly smaller than the nominal value of 0.707. Similarly, the TRK-I model provides a very small value of $M_{\rm h}$, a factor of $\sim$9 less than of the corresponding one-parameter model, while the resulting value $y = 6.14$ implies that $\Delta \simeq 10^6$, a value extremely large and unphysical. Finally, the MMRZ-I model provides again a very small value of M_h, while it is the only two-parameter model that fits the data worse than the corresponding one-parameter model. This is due to the fact that we have used $\kappa = 0.44$ and not $\kappa = 0.23$, which

Downloaded from https://academic.oup.com/mnras/article-abstract/422/1/106/1019897 by Instituto Nacional de Astrofisica, Optica y Electronica user on 25 October 2018

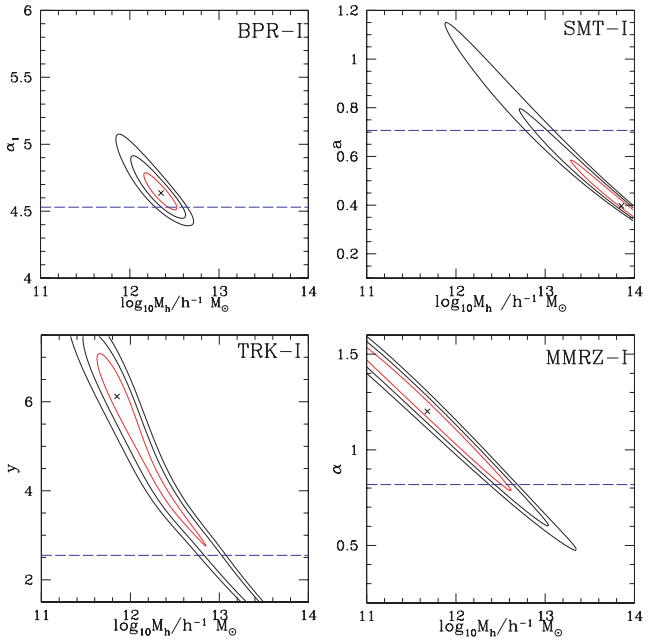

Figure 3. Contour plots of the two fitted parameter–solution space. The 1σ level is indicated by the relatively thicker red curve. The blue dashed line indicates the simulation-based value of the y-axis parameter.

is used in the one-free-parameter model, as suggested by MMRZ. Had we used the latter κ value we would have found an extremely small value of $M_{\rm h} \simeq 10^{10}\,h^{-1}\,{\rm M}_{\odot}$. These results probably indicate a degeneracy between the two fitted parameters, a fact which we indeed confirm for the SMT-I, TRK-I and MMRZ-I models, as can be seen in Fig. 3 where we plot the 1, 2 and 3σ likelihood contours in the parameter plane. In contrast to the above models, no such degeneracy is present for the BPR-I model. Note that in Fig. 3 the cross indicates the best two-parameter solution, while the dashed line indicates the simulation-based value of the second parameter. In the case of the TRK-I model, the latter corresponds to the virialization value ($y = \log_{10}355$), used in the one-free-parameter fit.

(iv) Beyond the previously mentioned fundamental flow of the two-parameter models (SMT-I, TRK-I and MMRZ-I), they all provide relatively comparable to the BPR-II model fits of the QSO bias data but only within the range $0.8 \lesssim z \lesssim 2.4$ (see the bottom panel of Fig. 2). Furthermore, the MMRZ-I model, as in the case of the one-free-parameter fit, provides an anti-biased value at $z \lesssim 0.2$, while it also provides the worst overall fit to the QSO bias data.

(v) Finally, the BPR one-parameter model scores the best among all the one- or two-free-parameter models and over the whole available QSO bias redshift range, while it is statistically equivalent to the BPR-I and BPR-II models (since $|\Delta{\rm AIC}_c| \lesssim 1.8$; see Table 3).

Table 3. Results of the pair difference $\Delta{\rm AIC}_c$ for the bias evolution models fitted to the optical QSO data.

	BPR-I	BPR-II	SMT	JING	TRK	MMRZ
BPR	−1.3	−1.8	−10.3	−5.1	−2.9	−7.3
BPR-I		−0.5	−9.0	−3.8	−1.6	−6.0
BPR-II			−8.5	−3.3	−1.1	−5.5
SMT				5.2	7.4	3.1
JING					2.2	−2.1
TRK						−4.3

We assess in a more quantitative manner the statistical relevance of the different theoretical bias models in representing the observational QSO bias data by using the information theory parameter $\rm AIC_c$ and presenting in Table 3 the model pair difference $\Delta{\rm AIC}_c$. As previously discussed a smaller $\rm AIC_c$ value indicates a model that better fits the data, while a small $|\Delta{\rm AIC}_c|$ value (i.e. $\lesssim$2) indicates that the two comparison models represent the data at a statistically equivalent level. Due to the resulting unphysical second free parameter, as discussed previously, we do not use in Table 3 a comparison based on the SMT-I, TRK-I and MMRZ-I models. It is obvious that the one-free-parameter BPR model fairs the best among the different models, while it is statistically equivalent, as indicated by the relevant values of $\Delta{\rm AIC}_c$, to the BPR-I and BPR-II models and to a slightly lesser degree to the TRK model.

4.2 Optical VVTS galaxy results

This model–data comparison takes place at relatively low redshifts ($z < 1.5$), covering a small dynamical range in z, and therefore we will use only the one-free-parameter models to fit the galaxy bias data. An additional reason is that even with the much larger z dynamical range covered by the QSO data, the second parameter could not be constrained (except for the case of the BPR-I and BPR-II models).

The results of the χ^2-minimization procedure are presented in Table 4, while in Fig. 4 we present the model fits to the galaxy bias data. Note that the layout of Fig. 4 is the same as Fig. 1. It is evident that the BPR model fairs the best providing the lowest reduced χ^2 and $\rm AIC_c$ parameter with respect to the other models, while the MMRZ model fairs the worst. However, due to the small dynamical range in redshift, the information theory pair model characterization parameter, $\Delta{\rm AIC}_c$, indicates that all the bias models are statistically equivalent in representing the bias data, since $\Delta{\rm AIC}_c \lesssim 1.8$ for any model pair. As in the QSO case, we provide an average halo mass that hosts VVTS optical galaxies using an $\rm AIC_c$ weighted procedure over the different one-parameter bias models. The resulting weighted mean and combined weighted standard deviation are

$$(\mu_{M_{\rm h}}, \sigma_{M_{\rm h}}) = (6.3, 2.1) \times 10^{11}\,h^{-1}\,{\rm M}_{\odot},$$

while the weighted scatter of the mean is also $\sim 0.9 \times 10^{11}\,h^{-1}\,{\rm M}_{\odot}$.

It is interesting to point out that the only model that finds that at $z = 0$ the optical galaxies are unbiased ($b_0 \simeq 1$), in agreement with other studies of wide-area optical galaxy catalogues (Lahav *et al.* 2002; Verde *et al.* 2002), is the BPR model, while all the other models indicate that optical galaxies are quite anti-biased with $b(0) \leq 0.9$.

Table 4. Results of the χ^2-minimization procedure between the one-free-parameter models and the optical VVTS galaxy bias data.

Model	$10^{11}\,h^{-1}\,{\rm M}_{\odot}$	$b(0)$	$\chi^2_{\rm min}$/d.o.f.	$\rm AIC_c$
BPR	6.0 ± 2.5	0.99	0.29/4	2.29
SMT	6.4 ± 1.9	0.90	0.45/4	2.45
JING	5.1 ± 1.3	0.83	0.93/4	2.93
TRK	7.8 ± 1.9	0.86	0.74/4	2.74
MMRZ	6.1 ± 1.3	0.70	2.10/4	4.10

Downloaded from https://academic.oup.com/mnras/article-abstract/422/1/106/1019897 by Instituto Nacional de Astrofisica, Optica y Electronica user on 25 October 2018

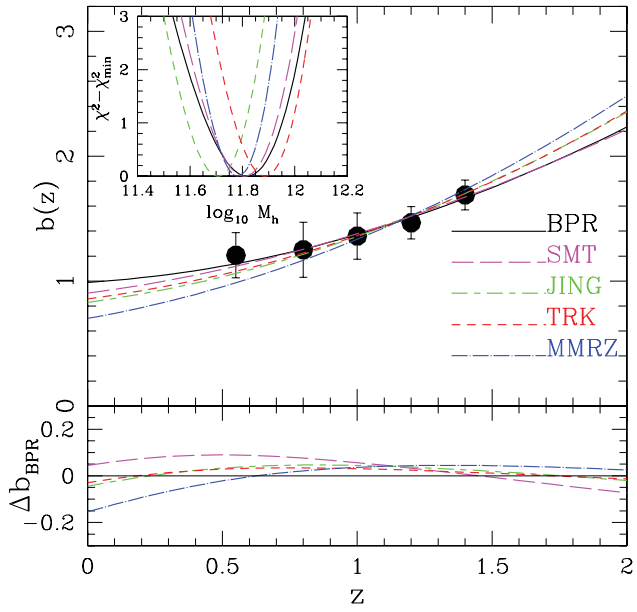

Figure 4. Results of the χ^2-minimization procedure between the VVTS galaxy bias data and the bias models with one free parameter.

5 CONCLUSIONS

In this work, we assess the ability of five recent bias evolution models to represent a variety of observational bias data, based either on optical QSOs or on optical galaxies. To this end we applied a χ^2-minimization procedure between the observational bias data, after rescaling them to the *WMAP7* cosmology, with the model expectations, through which we fit the model free parameters.

In performing this comparison, we assume that each halo is populated by one extragalactic mass tracer, being a QSO or a galaxy, an assumption that is justified since the observational data have been estimated on the basis of either the large-scale clustering ($>1\,h^{-1}$ Mpc), corresponding to the halo–halo term, or the corrected for non-linear effects variance of the smoothed (on $8\,h^{-1}$ Mpc scales) density field.

The comparison shows that all models fit at an acceptable level the QSO data as indicated by the their reduced χ^2 values. Using the information theory characteristic, AIC$_c$, which takes into account the different number of model free parameters, we find that the model that rates the best among all the others is the Basilakos & Plionis (2001, 2003) model with the tracer merging extension of BPR, which is the only model fitting accurately the optical QSO bias data over the whole redshift range traced ($0 < z < 4$). The only other model that is statistically equivalent at an acceptable level is that of TRK. The average, over the different bias models, DM halo mass that hosts optical QSOs is $M_{\rm h} \simeq 2.7(\pm 0.6) \times 10^{12}\,h^{-1}\,{\rm M}_{\odot}$.

Finally, all the investigated bias models fit well and at a statistically equivalent level the VVTS galaxy bias data, with the BPR model scoring again the best, and the MMRZ model the worst. The average, over the different bias models, DM halo mass hosting optical galaxies is $M_{\rm h} \simeq 6(\pm 2) \times 10^{11}\,h^{-1}\,{\rm M}_{\odot}$.

ACKNOWLEDGMENTS

SB wishes to thank the Department ECM of the University of Barcelona for hospitality, and acknowledges financial support from the Spanish Ministry of Education, within the programme of Estancias de Profesores e Investigadores Extranjeros en Centros Españoles (SAB2010-0118).

REFERENCES

Akaike H., 1974, IEEE Trans. Autom. Control, AC-19, 716
Bagla J. S., 1998, MNRAS, 299, 417
Bardeen J. M., Bond J. R., Kaiser N., Szalay A. S., 1986, ApJ, 304, 15
Basilakos S., Plionis M., 2001, ApJ, 550, 522
Basilakos S., Plionis M., 2003, ApJ, 593, L61
Basilakos S., Plionis M., Ragone-Figueroa C. R., 2008, ApJ, 678, 627 (BPR)
Basilakos S., Plionis M., Pouri A., 2011, Phys. Rev. D, 83, 123525
Bertschinger E., 2001, ApJS, 137, 1
Cole S., Kaiser N., 1989, MNRAS, 237, 1127
Croom S. M., et al., 2005, MNRAS, 356, 415
Davis M., Peebles P. J. E., 1983, ApJ, 267, 465
Davis T. M., et al., 2007, ApJ, 666, 716
de Simon A., Maggiore M., Riotto A., 2011, MNRAS, 412, 2587
Eisenstein D. J., Hu W., 1998, ApJ, 496, 605
Fry J. N., 1996, ApJ, 461, L65
Godlowski W., Szydlowski M., 2005, Phys. Lett. B, 540, 1
Hamana T., Yoshira N., Suto Y., 2002, ApJ, 568, 455
Hamilton, A. J. S., 1998, Linear Redshift Distortions: A Review. Kluwer, Dordrecht, p. 185
Hui L., Parfrey K. P., 2008, Phys. Rev. D, 77, 043527
Jing Y. P., 1998, ApJ, 503, L9 (JING)
Kaiser N., 1984, ApJ, 284, L9
Kaiser N., 1987, MNRAS, 227, 1
Komatsu E., et al., 2011, ApJS, 192, 18
Lahav O., et al., 2002, MNRAS, 333, 961
Liddle A. R., 2004, MNRAS, 351, L49
Linder E. V., 2005, Phys. Rev. D, 72, 043529
Ma C.-P., Maggiore M., Riotto A., Jun Z., 2011, MNRAS, 411, 2644 (MMRZ)
Maggiore M., Riotto A., 2010, ApJ, 711, 907
Manera, M., Gaztanaga, E., 2011, MNRAS, 415, 383
Manera M., Sheth R. K., Scoccimarro R., 2009, MNRAS, 402, 589
Marinoni C., et al., 2005, A&A, 442, 801
Matarrese S., Coles P., Lucchin F., Moscardini L., 1997, MNRAS, 286, 115
Mo H. J., White S. D. M., 1996, MNRAS, 282, 347
Mo H. J., Jing Y. P., White S. D. M., 1997, MNRAS, 284, 189
Moscardini L., Coles P., Lucchin F., Matarrese S., 1998, MNRAS, 299, 95
Myers A. D., et al., 2006, ApJ, 658, 85
Nusser A., Davis M., 1994, ApJ, 421, L1
Pillepich A., Porciani C., Han O., 2010, MNRAS, 402, 191
Press W. H., Schechter P., 1974, ApJ, 187, 425
Ragone-Figueroa C., Plionis M., 2007, MNRAS, 377, 1785
Ross N. P., et al., 2009, ApJ, 697, 1634
Saini T. D., Weller J., Bridle S. L., 2004, MNRAS, 348, 603
Schaefer B. M., Douspis M., Aghanim N., 2009, MNRAS, 397, 925
Seljak U., Warren M. S., 2004, MNRAS, 355, 129
Shen Y., et al., 2009, ApJ, 697, 1656
Sheth R. K., Tormen G., 1999, MNRAS, 308, 119
Sheth R. K., Mo H. J., Tormen G., 2001, MNRAS, 323, 1 (SMT)
Simon P., 2005, A&A, 430, 827
Springel V., 2005, MNRAS, 364, 1105
Sugiura N., 1978, Commun. Stat. – Theory Methods, 7, 13
Sugiyama N., 1995, ApJS, 100, 281
Tegmark M., Peebles P. J. E., 1998, ApJ, 500, L79
Tinker J. L., Weinberg D. H., Zheng Z., 2005, ApJ, 631, 41
Tinker J. L., Robertson B. E., Kravtsov A. V., Klypin A., Warren M. S., Yepes G., Gottlober S., 2010, ApJ, 724, 878 (TRK)
Valageas P., 2009, A&A, 508, 93
Valageas P., 2011, A&A, 525, 98
Verde L., et al., 2002, MNRAS, 335, 432

Downloaded from https://academic.oup.com/mnras/article-abstract/422/1/106/1019897 by Instituto Nacional de Astrofisica, Optica y Electronica user on 25 October 2018

Wang L., Steinhardt J. P., 1998, ApJ, 508, 483
Weinberg N. N., Kamionkowski M., 2003, MNRAS, 341, 251

APPENDIX A: SIMULATION BASED BPR MODEL PARAMETER ESTIMATION

A1 ΛCDM simulations

We have run a new *WMAP7* ΛCDM *N*-body simulation using the GADGET-2 code (Springel 2005) with DM only. The size of the box simulation is $500h^{-1}$ Mpc and the number of particles is 512^3. The adopted cosmological parameters are the following: $\Omega_{\rm m} = 0.273$, $\Omega_\Lambda = 0.727$, $h = 0.704$, $\sigma_8 = 0.81$ and the particle mass is $7.07 \times 10^{10}\, h^{-1}\, {\rm M}_\odot$, comparable to the mass of a single galaxy. The initial conditions were generated using the GRAFIC2 package (Bertschinger 2001). We also use a similar size simulation, generated in Ragone-Figueroa & Plionis (2007), of a ΛCDM model with $\Omega_{\rm m} = 0.3$, $\Omega_\Lambda = 0.7$, $h = 0.72$ and $\sigma_8 = 0.9$.

The DM haloes were defined using a FoF algorithm with a linking length $l = 0.17\langle n\rangle^{-1/3}$, where $\langle n\rangle$ is the mean particle density.

We estimate the bias redshift evolution of the different DM haloes, with respect to the underlying matter distribution, by measuring their relative fluctuations in spheres of radius $8\ h^{-1}$ Mpc, according to the definition of equation (3), that is,

$$b(M, z) = \frac{\sigma_{8,\rm h}(M, z)}{\sigma_{8,\rm m}(z)}\ , \tag{A1}$$

where the subscripts 'h' and 'm' denote haloes and the underlying mass, respectively. The values of $\sigma_{8,\rm h}(M, z)$, for haloes of mass M, are computed at different redshifts, z, by

$$\sigma^2_{8,\rm h}(M, z) = \left\langle \left(\frac{N - \bar{N}}{\bar{N}} \right)^2 \right\rangle - \frac{1}{\bar{N}}\ , \tag{A2}$$

where $\bar{N}$ is the mean number of such haloes in spheres of $8\ h^{-1}$ Mpc radius and the factor $1/\bar{N}$ is the expected Poissonian contribution to the value of $\sigma^2_{8,\rm h}$. Similarly, we estimate at each redshift the value of the underlying mass $\sigma_{8,\rm m}$. In order to numerically estimate $\sigma^2_{8,j}$ we randomly place $N_{\rm rand}$ sphere centres in the simulation volume, such that the sum of their volumes is equal to ∼1/8 the simulation volume ($N_{\rm rand} = 8000$). This is to ensure that we are not oversampling the available volume, in which case we would have been multiply sampling the same halo or mass fluctuations. The relevant uncertainties are estimated as the dispersion of $\sigma^2_{8,j}$ over 20 bootstrap re-samplings of the corresponding halo sample. Note that we do not explicitly correct for possible non-linear effects in δ (although the density field is indeed smoothed on linear scales – $8\ h^{-1}$ Mpc); we do, however, expect that such effects should be mostly cancelled in the overdensity ratio definition of the bias.

We use the DM halo bias evolution, measured in the two simulations, for different DM halo mass range subsamples in order to constrain the constants of our bias evolution model, that is, $\mathcal{C}_1, \mathcal{C}_2$. The procedure used is based on a χ^2 minimization of whose details are presented in BPR and thus will not be repeated here. In Fig. A1, we present as points the simulation-based values of these parameters, for both cosmologies used, and as continuous curves their analytic fits, which are given in equations (20) and (21). The resulting values of the parameters $\alpha_{1,2}$ and $\beta_{1,2}$ can be found in Table A1. It is interesting to note that the slope of the functions $\mathcal{C}_1$ and $\mathcal{C}_2$ is roughly a constant and independent of cosmology, with a value $\beta_1 \simeq \beta_2 \simeq 0.35(\pm 0.06)$.

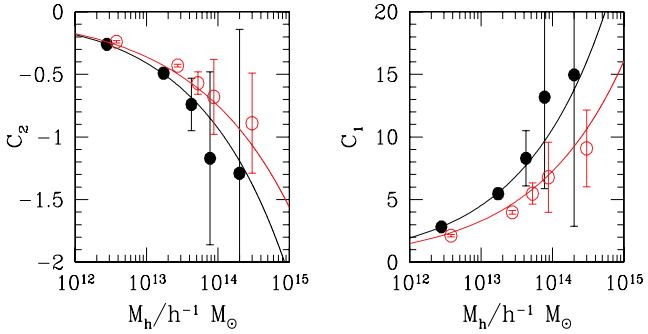

Figure A1. The parameters $\mathcal{C}_1$ and $\mathcal{C}_2$ derived from the *WMAP7* (filled points) and *WMAP1* (open circles) ΛCDM simulations (filled circles). The continuous lines correspond to the function form of equation (A3), with best-fitting parameters shown in Table A1.

Table A1. Results of the χ^2 minimization used to evaluate the parameters that enter in the $\mathcal{C}_1$ and $\mathcal{C}_2$ constants (which depend on DM halo mass) of the BPR bias evolution model.

Model	α_1	α_2	β_1	β_2
WMAP1	3.30 ± 0.13	-0.36 ± 0.01	0.34 ± 0.04	0.32 ± 0.04
WMAP7	4.53 ± 0.22	-0.41 ± 0.02	0.37 ± 0.04	0.36 ± 0.04

A2 Dependence of the BPR model constants on cosmology

The dependence of the constants α_1 and α_2 of the BPR bias model on the different cosmological parameters is an important prerequisite for the versatile use of the model in investigating the bias evolution of different mass tracers and determine the mass of the DM haloes which they inhabit. In Basilakos & Plionis (2001) we predicted a power-law dependence of α_2 on $\Omega_{\rm m}$. Indeed, fitting such a dependence, using the *WMAP1* and *WMAP7* ΛCDM simulations, we find

$$\alpha_2(\Omega_{\rm m}) = -0.41 \left(\frac{0.273}{\Omega_{\rm m}} \right)^n \quad \text{with} \quad n \simeq 2.8/2 \tag{A3}$$

consistent with the value $n = 3/2$ anticipated in Basilakos & Plionis (2001).

Now, in order to investigate the dependence on different cosmological parameters of the parameter a_1, we have used the optical QSO data and the procedure outlined in Section 2.2 to scale the QSO bias data to different flat cosmologies, using a grid of $\Omega_{\rm m}$ and σ_8 values. The grid was defined as follows: $\Omega_{\rm m} \in [0.18, 0.5]$ and $\sigma_8 \in [0.7, 0.94]$, both in steps of 0.01. We then minimize the BPR bias evolution model to the scaled QSO bias values to different cosmologies, finally providing for each pair of $(\Omega_{\rm m}, \sigma_8)$ values the best-fitted α_1 and $M_{\rm h}$ values.

Then using a trial-and-error approach to select the best functional dependence of the derived $\alpha_1(\Omega_{\rm m}, \sigma_8)$ values to the relevant cosmological parameters, we find a best-fitting model of the form

$$\alpha_1(\Omega_{\rm m}, \sigma_8) \simeq 4.53 \left(\frac{0.81}{\sigma_8} \right)^{\kappa_1} \exp\left[\kappa_2(\Omega_{\rm m} - 0.273)\right] \tag{A4}$$

with

$$(\kappa_1, \kappa_2) = \begin{cases} (12.15, 0.30) & \Omega_{\rm m} \le 0.273 \\ (8.70, 0.37) & \Omega_{\rm m} > 0.273 \end{cases} \tag{A5}$$

In Fig. A2, we correlate the derived $\alpha_1(\Omega_{\rm m}, \sigma_8)$ values, resulting from fitting the BPR bias evolution model to the scaled QSO bias

Downloaded from https://academic.oup.com/mnras/article-abstract/422/1/106/1019897 by Instituto Nacional de Astrofisica, Optica y Electronica user on 25 October 2018

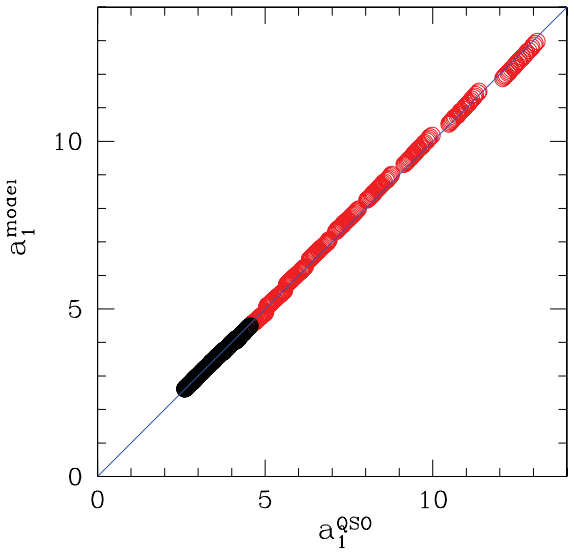

Figure A2. Correlation between (i) the best-fitted α_1 values of the BPR model using the QSO bias data scaled to different cosmologies for a grid of Ω_m and σ_8 values and (ii) the predicted α_1 values, based on equation (A4). The red points correspond to $\Omega_m \leq 0.273$, while the black points to $\Omega_m > 0.273$.

data, to those predicted by the model of equation (A4). It is evident that the correspondence is excellent, indicating that indeed the above-estimated cosmological dependence of α_1 is the indicated one.

This paper has been typeset from a TEX/LATEX file prepared by the author.

Downloaded from https://academic.oup.com/mnras/article-abstract/422/1/106/1019897 by Instituto Nacional de Astrofisica, Optica y Electronica user on 25 October 2018